

LETTER TO THE EDITOR

A detailed non-LTE analysis of LB-1: Revised parameters and surface abundances

S. Simón-Díaz^{1,2}, J. Maíz Apellániz³, D. J. Lennon^{1,2}, J. I. González Hernández^{1,2}, C. Allende Prieto^{1,2}, N. Castro⁴,
A. de Burgos⁵, P. L. Dufton⁶, A. Herrero^{1,2}, B. Toledo-Padrón^{1,2}, S. J. Smartt⁶

(Affiliations can be found after the references)

Received xxx; accepted xxx

ABSTRACT

Context. LB-1 has recently been proposed to be a binary system at 4 kpc consisting of a B-type star of $8 M_{\odot}$ and a massive stellar black hole (BH) of $70 M_{\odot}$. This finding challenges our current theories of massive star evolution and formation of BHs at solar metallicity.

Aims. Our objective is to derive the effective temperature, surface gravity and chemical composition of the B-type component in order to determine its nature and evolutionary status and, indirectly, to constrain the mass of the BH.

Methods. We use the non-LTE stellar atmosphere code FASTWIND to analyse new and archival high resolution data.

Results. We determine (T_{eff} , $\log g$) values of ($14\,000 \pm 500$ K, 3.50 ± 0.15 dex) that, combined with the *Gaia* parallax, implies a *spectroscopic* mass, from $\log g$, of $3.2^{+2.1}_{-1.9} M_{\odot}$ and an *evolutionary* mass, assuming single star evolution, of $5.2^{+0.3}_{-0.6} M_{\odot}$. We determine an upper limit of 8 km s^{-1} for the projected rotational velocity and derive the surface abundances, finding the star to have a silicon abundance below solar, to be significantly enhanced in nitrogen and iron, and depleted in carbon and magnesium. Complementary evidence derived from a photometric extinction analysis and *Gaia* yields similar results for T_{eff} and $\log g$ and a consistent distance around 2 kpc.

Conclusions. We propose that the B-type star is a slightly evolved main sequence star of $3-5 M_{\odot}$ with surface abundances reminiscent of diffusion in late B/A chemically peculiar stars with low rotational velocities. There is also evidence for CN-processed material in its atmosphere. These conclusions rely critically on the distance inferred from the *Gaia* parallax. The goodness of fit of the *Gaia* astrometry also favours a high-inclination orbit. If the orbit is edge-on and the B-type star has a mass of $3-5 M_{\odot}$, the mass of the dark companion would be $4-5 M_{\odot}$, which would be easier to explain with our current stellar evolutionary models.

Key words. techniques: spectroscopic, binaries: spectroscopic, stars: black holes, stars: early-type, stars: fundamental parameters, stars: abundances

1. Introduction

The LAMOST collaboration has recently announced the potential discovery of a black-hole (BH) in the system LB-1 (LS V +22 25, ALS 8775) of about $70 M_{\odot}$ (Liu et al. 2019). The object is part of a wide binary system in which the visible component is an extremely narrow lined B-type star. The mass determination of the dark companion is based on three key empirical measurements. First, the radial velocity curve of the B-type star, which allowed identification of the period ($P = 78.9 \pm 0.3$ d) and the mass function ($PK_{\text{B}}/2\pi G = 1.20 \pm 0.05 M_{\odot}$, with $K_{\text{B}} = 52.8 \pm 0.7 \text{ km s}^{-1}$) of the binary system. Second, the mass of the B-type star, which was proposed to be $8.2^{+0.9}_{-1.2} M_{\odot}$. Finally, the authors measure changes in radial velocity associated with the broad and strong $H\alpha$ emission line which they suggest are associated with a Keplerian disc orbiting the black hole. If correct this discovery would have important implications for stellar evolution (Groh et al. 2019; Belczynski et al. 2019; Shen et al. 2019).

Since then, however, it has been shown that the radial velocity measurements of the $H\alpha$ emission line are spurious (El-Badry & Quataert 2019; Abdul-Masih et al. 2019), resulting from the influence of the underlying broad stellar absorption typical of late main-sequence B-type stars. This was not taken into account by Liu et al. (2019). Eldridge et al. (2019) further propose, based on BPASS binary evolution models, that a more likely scenario is a BH mass around $4-7 M_{\odot}$, and that the distance implied by the *Gaia* parallax is correct. This distance is almost a factor of

two smaller than that inferred by Liu et al. when assuming that the mass of the B-star was $8.2 M_{\odot}$.

In this letter we focus on a detailed non-LTE quantitative spectroscopic analysis of a set of high quality spectra to determine the stellar parameters, including the so-called evolutionary and spectroscopic masses, and chemical composition of the B-type star. Our ultimate aim is to check for consistency with the currently evolving picture of LB-1 as a typical, though extremely interesting, B+BH (B-type star plus black hole) system at a distance of approximately 2 kpc. In section 2 we discuss the observational data. In section 3 we present our analysis and results, and in section 4 we discuss some implications.

2. Observations

On November 4 and 5, 2019, we obtained two 1800 s exposures with the HARPS-N@TNG3.5 m échelle spectrograph. Spectral resolution (R) is 115 000 with wavelength coverage from 383 to 690 nm. The signal-to-noise ratio (S/N) per pixel in the blue spectral ranges from 35 to 70 in the co-added and re-binned ($0.05 \text{ \AA}/\text{pixel}$) spectrum.

On November 30 2019, we also obtained a set of five 15-minute, $R = 25\,000$ spectra with the HORuS@GTC10.4 m échelle spectrograph, which provides nearly complete spectral coverage between 380 and 690 nm. The combined HORuS spec-

trum¹ has a median S/N per pixel (1/3 of a resolution element) of 150 (210 at 500 nm).

We also downloaded the raw HIRES ($R \sim 50\,000$) data presented by Liu et al. (2019) from the Keck archive and used standard IRAF procedures to re-reduce the 600s single exposure from 24 December 2017 (the highest S/N spectrum from the HIRES dataset). During the reduction process, no flat-fielding was applied since this does not improve the S/N of the extracted spectrum and causes further problems in normalising the orders which contain broad Balmer lines.

Last, we downloaded all 12 publicly available LAMOST spectra from DR5v3. The standard flux calibrated pipeline products were normalized for comparison with the other high resolution, non flux calibrated spectra (see below and Appendix A).

In comparing model spectra and observed line profiles all data must be appropriately normalized. However, the blaze correction and normalization of those individual orders in an échelle spectrum that includes broad and extended lines (as is the case of the Balmer lines in late B-type or A-type stars) is difficult. Even a small misplacement of the continuum can significantly distort the shape of the far line-wings, that are the most reliable indicators of surface gravity. This reliance on the line wings is even more important for LB-1 as there is clearly emission effecting the intensity of the Balmer line cores. We refer the reader to Appendix A for a more technical discussion of this aspect of our analysis.

3. Stellar parameters and surface abundances of the B-type star in LB-1

3.1. Spectroscopic parameters

As a first step in our analysis we used a grid of standards for spectral classification of OB stars to determine the spectral type and luminosity class of LB-1 (see Appendix B). We obtain B6 IVe, a later spectral type that implies a substantially cooler effective temperature than that obtained by Liu et al. (2019). We also checked in the three high resolution spectra for signatures of a hidden fast rotating B-type star which could be associated with the strong H_α emission through a Be star phenomenon, but we did not find any.

To perform the quantitative spectroscopic analysis, including the determination of the projected rotational velocity ($v \sin i$), the spectroscopic parameters (T_{eff} , $\log g$) and the abundance analysis, we used the IACOB-BROAD tool (Simón-Díaz & Herrero 2014) and a grid of synthetic spectra obtained with the non-LTE, line-blanketed, spherical stellar atmosphere code FASTWIND (Puls et al. 2005).

The IACOB-BROAD analysis of the $\text{Si II } \lambda 6371 \text{ \AA}$ line leads to an upper limit in $v \sin i$ of 8 km s^{-1} , a result that is also supported by the fact that the two components of the $\text{Mg II } \lambda \lambda 4481.126, 4481.325 \text{ \AA}$ doublet can be resolved in the HARPS-N spectrum. The analysis of other lines gives a similar result. In all cases we find that the profiles cannot be properly fitted with a pure rotational profile, indicating that there is some additional broadening affecting the line, and hampering a proper determination of $v \sin i$ below the proposed value.

Due to the very low $v \sin i$ of LB-1, and the high S/N of the data, we can securely measure extremely weak lines such as the $\text{Si III } \lambda \lambda 4552, 4567 \text{ \AA}$ lines, that have equivalent widths of roughly 11 and 8 mÅ respectively (correcting the former for a

¹ Individual spectra were reduced with the HORuS chain: github.com/callendeprieto/chain.

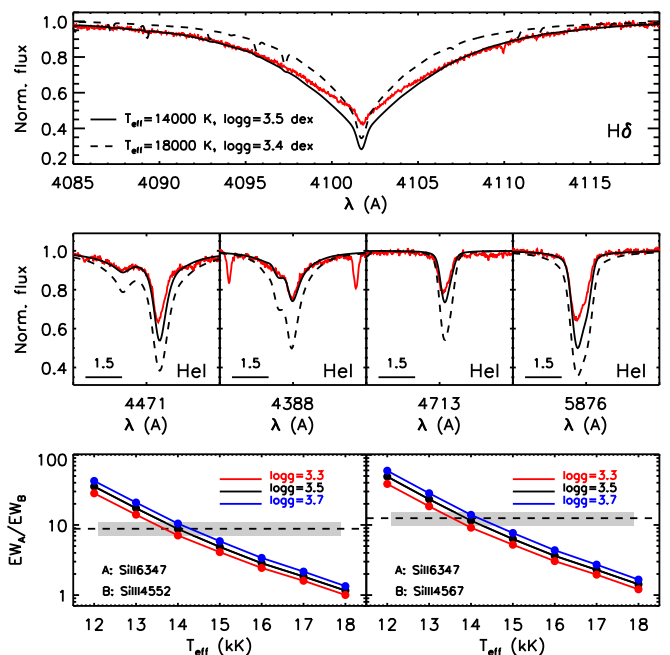


Fig. 1. Summary of the quantitative spectroscopic analysis strategy we follow for the determination of T_{eff} and $\log g$. Top and middle panels show line profiles of $\text{H}\delta$ and some He I lines in the HIRES spectrum, respectively. Solid and dashed lines in these panels depict the synthetic spectra associated with two FASTWIND models with a different (T_{eff} , $\log g$) pair: our best solution (14 000 K, 3.5 dex, solid) and the one proposed by Liu et al. (2019) (18 000 K, 3.4 dex, dashed). Note that $\text{H}\delta$ and some He I lines show infilling from the disk emission. Bottom panels show the predicted variation of the $\text{Si II } \lambda 6347/\text{Si III } \lambda 4552$ (left) and $\text{Si II } \lambda 6347/\text{Si III } \lambda 4567$ (right) ratios with T_{eff} for three values of $\log g$ (Si abundance fixed to solar). The horizontal grey band indicates the empirical measurement and its associated uncertainty.

blend with a Si II line). Hence, we are able to use the $\text{Si II}/\text{Si III}$ ionization equilibrium (together with the fitting of the wings of some of the Balmer lines, see below) to estimate the effective temperature of the star (see Fig. 1). Our estimate for this parameter is $14\,000 \pm 500 \text{ K}$, which is in fairly good agreement with the value obtained by Abdul-Masih et al. (2019), but 4 000 K less than that proposed by Liu et al. (2019).

In addition, several He I lines are used as a consistency check of the temperature as well as to have information about the helium abundance, having in mind that some of these lines (like $\text{He I } \lambda \lambda 4471$ and 5875 \AA , see middle panels in Fig. 1) may be contaminated by emission from the disk, whose nature – circumbinary or circumstellar – is still unknown (El-Badry & Quataert 2019; Abdul-Masih et al. 2019). The good fit to the other He I lines for the derived T_{eff} indicates that the helium abundance of the star is $\text{N}(\text{He})/\text{N}(\text{H}) = 0.1$ (*i.e.* normal).

Gravity is constrained at the same time as T_{eff} using the wings of the Balmer lines, specially $\text{H}\delta$ and $\text{H}\gamma$, since $\text{H}\beta$ and $\text{H}\alpha$ are significantly contaminated by the strong disc emission. The derived value of $\log g$ is 3.50 ± 0.15 dex and we show our final fit of the $\text{H}\delta$ profile in Fig. 1. We also compare a FASTWIND model for the T_{eff} and $\log g$ determined by Liu et al. (2019). As can be seen, the combination of effective temperature and gravity estimated by these authors results in a poor fit to the wings of the Balmer lines. The reason is likely due to some form of processing (e.g. flat-fielding and illumination corrections combined with the strong blaze function of the orders) of the Keck spectrum which significantly affects the normalization of the Balmer

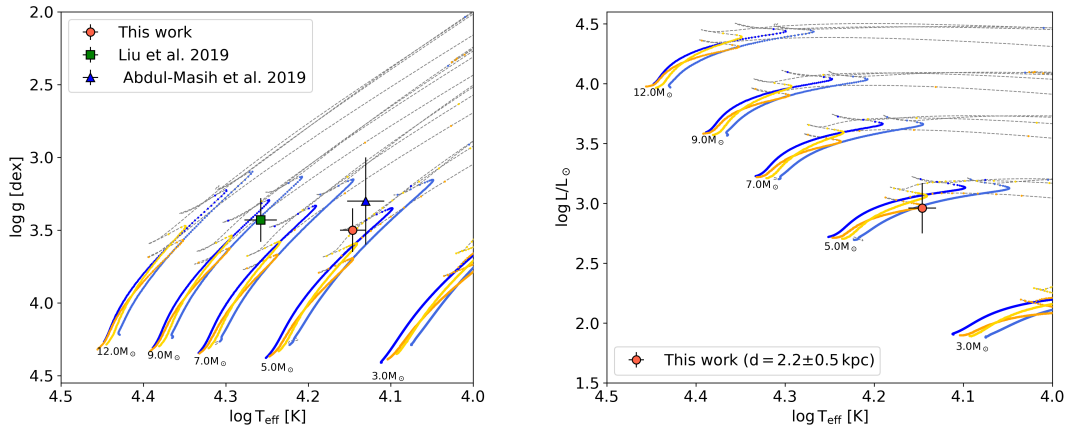


Fig. 2. Location of the B star component of the LB-1 system in the Kiel (left) and HR (right) diagrams. The various evolutionary tracks correspond to models with and without rotation from Ekström et al. (2012, orange) and Brott et al. (2011, blue). In the Kiel diagram we also indicate the location of the star accordingly to the parameters derived by Liu et al. (2019) and Abdul-Masih et al. (2019). In the HR diagram we show the position of the star assuming the Gaia distance computed in Appendix D.

Table 1. Summary of spectroscopic and fundamental parameters resulting from the quantitative spectroscopic analysis of the late-B star in the LB-1 system. Stellar radius, luminosity and spectroscopic mass have been computed assuming a distance to the star $d = 2.2 \pm 0.5$ kpc, and an extinction $A_V = 1.503 \pm 0.027$ mag. Evolutionary mass obtained with BONNSAI (Schneider et al. 2014) using T_{eff} , $\log g$, and $\log L$ as input parameters. Abundances have been obtained assuming fixed values of T_{eff} (14 000 K), $\log g$ (3.5 dex), helium abundance ($N_{\text{He}}/N_{\text{H}} = 0.1$), and microturbulence (1 km s^{-1}). Last column refers to the abundances derived in B-type stars in the Orion OB1 association Nieva & Simón-Díaz (2011), which can be considered as the present-day abundances of the solar neighborhood up to a few kpc.

| Spectroscopic parameters | | Fundamental parameters | | Surface abundances (LB-1) | | Ref. abund. | |
|--------------------------|-----------------------|------------------------|-------------------------------------|---------------------------|-----------------------|-----------------|-------|
| $T_{\text{eff}} =$ | $14\,000 \pm 500$ [K] | $R =$ | 5.3 ± 1.2 [R_{\odot}] | $\epsilon(\text{Si}) =$ | 7.20 ± 0.15 [dex] | 7.50 ± 0.06 | [dex] |
| $\log g =$ | 3.5 ± 0.15 [dex] | $\log(L/L_{\odot}) =$ | 2.98 ± 0.21 [dex] | $\epsilon(\text{Mg}) =$ | 6.87 ± 0.15 [dex] | 7.57 ± 0.06 | [dex] |
| $v \sin i =$ | < 10 [km/s] | $M_{\text{sp}} =$ | $3.2^{+2.1}_{-1.9}$ [M_{\odot}] | $\epsilon(\text{C}) =$ | 7.50 ± 0.2 [dex] | 8.35 ± 0.03 | [dex] |
| $Y_{\text{He}} =$ | 0.1 | $M_{\text{ev}} =$ | $5.2^{+0.3}_{-0.6}$ [M_{\odot}] | $\epsilon(\text{N}) =$ | 8.20 ± 0.15 [dex] | 7.82 ± 0.07 | [dex] |

lines if not done carefully (see Appendix A), plus their overestimate of T_{eff} which is too high to fit the Si III/Si II ionization equilibrium.

3.2. Fundamental parameters

By locating the star in the Kiel diagram (Fig. 2, left) and comparing with different evolutionary tracks for massive single stars (Ekström et al. 2012; Brott et al. 2011) we derive an evolutionary mass² (M_{ev}) of $\sim 5 M_{\odot}$. This should be compared with the value $8.2 M_{\odot}$ from Liu et al. and the lower estimate of $4.2^{+0.8}_{-0.7} M_{\odot}$ from Abdul-Masih et al. (2019). The main reason of this reduction by 40-50% from the evolutionary mass estimation by Liu et al. (2019) is the lower T_{eff} obtained in this work, and in Abdul-Masih et al. (2019).

An alternative estimate of the mass of the B-type star, its spectroscopic mass, can be derived from $\log g$ and the stellar radius (R), the later being determined from the observed spectral energy distribution (SED) and distance. Assuming the distance derived from the Gaia parallax ($2.20^{+0.49}_{-0.35}$ kpc, see Appendix D) and using the IDL tool CHORIZOS to estimate the extinction ($A_V = 1.503 \pm 0.027$ mag, see Appendix C) we obtain an absolute visual magnitude $M_V = -1.6 \pm 0.5$ mag. Note that the dominant uncertainty is the one coming from the distance. By fitting the synthetic SED of the best fitting FASTWIND model to this value

of M_V , we derive a radius of $5.3 \pm 1.2 R_{\odot}$ and, hence, using our derived T_{eff} and $\log g$, a luminosity $\log L/L_{\odot} = 2.98 \pm 0.21$ and a spectroscopic mass $M_{\text{sp}} = 3.2^{+2.1}_{-1.9} M_{\odot}$.

We can then use the derived luminosity to locate the star in the HR diagram (Fig. 2, right). In this case, the derived evolutionary mass is $\sim 5 M_{\odot}$, similar to that obtained from the Kiel diagram. Clearly there is a mismatch between evolutionary/Kiel masses and the spectroscopic mass, though we can rule out much lower masses, such as might be relevant to a post-AGB scenario as that would require a much lower surface gravity, inconsistent with the observations. However we have implicitly assumed a normal single star evolutionary scenario, which may not be valid for this object. An analysis with CHORIZOS where T_{eff} is derived from the photometry yields similar results (Appendix C).

As discussed in more detail in Appendix D, this range of masses for the B-type star, together with the apparent lack of motion in Gaia, are all consistent with a hypothesis of a high inclination system, implying a BH mass of only $3.8\text{--}4.9 M_{\odot}$. In that case the B-type star either has its rotation axis almost perpendicular to its orbital axis, or its rotational velocity is intrinsically very small.

3.3. Surface abundances

Due to the high S/N of our the data and low $v \sin i$ of the star we can reliably measure equivalent widths (EW s) for lines of $10 \text{ m}\text{\AA}$ or less. Figure 3 summarizes the EW measurements for a representative set of lines of the various ions indicated above

² This mass estimate assumes that the star is on (or close to) the main sequence and its evolution has not been affected by its companion, which might not be necessarily the case (see Eldridge et al. 2019).

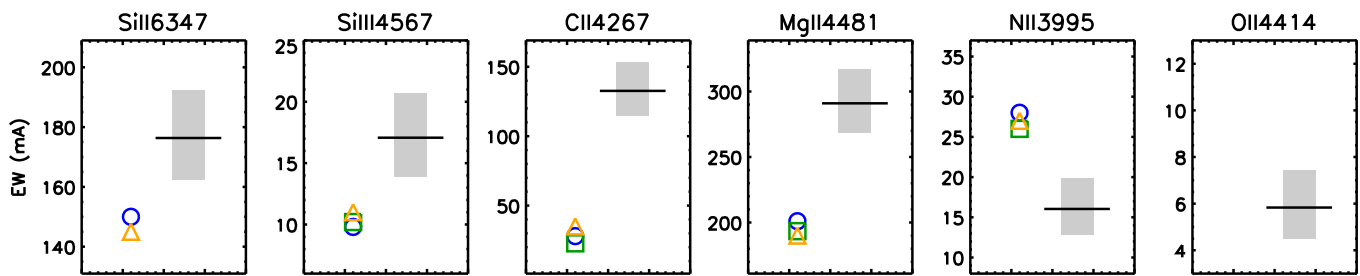


Fig. 3. Open symbols: EW measurements for the indicated diagnostic lines using the various high resolution spectra available (circles: HIRES; triangles: HARPS-N; squares: HORuS). Grey rectangles: Predicted range of EW s from FASTWIND models with the same T_{eff} and $\log g$ and a range in abundance ± 0.15 dex around the reference value (solid horizontal line, see Table 1). Right panel, including the predicted EW of the $O\text{ II } \lambda 4414$ Å has been included for reference, to indicate that the non detection of $O\text{ II}$ lines does not necessarily imply a low oxygen abundance.

for which we were able to determine abundances (i.e., those elements included in our FASTWIND computations). The figure presents a comparison of the empirical EW s with those predicted by our FASTWIND grid of models for fixed values of effective temperature (14 000 K), surface gravity (3.5 dex), helium abundance ($N_{\text{He}}/N_{\text{H}} = 0.1$), and microturbulence (1 km s^{-1}) and abundances covering a range ± 0.15 dex around the reference abundances, corresponding to B-type stars in the Orion OB1 association (see Table 1). The narrowness of the metal lines constrains the microturbulence to less than 3 km s^{-1} but we note that the abundance estimates are sensitive to the adopted value; for example increasing the microturbulence from 1 to 3 km s^{-1} , decreases the N abundance estimates by 0.1–0.2 dex.

The outcome of this abundance analysis is summarized in Table 1. In brief, we find that (1) the star has a silicon abundance that is 0.3 dex below the reference one; (2) carbon and magnesium surface abundances are depleted by more than a factor 7 and 5, respectively; and (3) nitrogen is enhanced by a factor ~ 2.5 . In addition, we note that, despite the high S/N ratio of the HIRES and HORuS spectra, we have not been able to detect the $O\text{ II } \lambda 4414$ Å line, one of the strongest $O\text{ II}$ lines in the optical spectrum; however, this does not necessarily imply a low oxygen abundance provided the small EW predicted by FASTWIND (see Fig. 3). Last, the FASTWIND synthetic spectra do not include iron lines. However, comparison of the observed Fe II spectrum with those predicted by TLUSTY models in the Bstar grid (Lanz & Hubeny 2007) implies that iron is enhanced in this star by $\sim 0.15\text{ dex}^3$.

4. Concluding remarks

There is no doubt that the spectrum of the B-type star is peculiar in a number of ways. Its projected rotational velocity is very small, $v \sin i < 8\text{ km s}^{-1}$, and if we accept that the high inclination angle implied by the disk applies to the B-star then the stellar rotational velocity is also very small. If the BH is the result of an interacting binary evolution scenario (Eldridge et al. 2019) then such a scenario must explain the small rotational velocity. The surface composition is also peculiar. The overabundance of N and depletion of C implies contamination with CN processed material, yet the depletion of Mg and enhancement of Fe are reminiscent of diffusion abundance patterns that are common in late B-type stars with low rotational velocities (Hempel & Holweger 2003). The system is also rather isolated and while its proper motion properties are normal, the systemic

radial velocity ($+28.9\text{ km s}^{-1}$) implies an LSR velocity of approximately $+16.4\text{ km s}^{-1}$ (using the solar peculiar motion from Schönrich et al. 2010). The star is almost directly anti-centre so this is mildly peculiar, for example direct measurements of massive star forming regions in this part of the Milky Way have LSR velocities of less than $\pm 10\text{ km s}^{-1}$ (Reid et al. 2014). This peculiar velocity may be the signature of a kick from the formation of the BH. Finally it is strange that there are no apparent signs of the motion of the B star around the dark companion in the *Gaia* data, and we propose a hypothesis that requires a near edge-on orbit, in which case the dark companion would have a mass as low as $4\text{--}5 M_{\odot}$, an order of magnitude lower than the Liu et al. (2019) value (Appendix D).

Acknowledgements. We thank J. Hernández for his help with *Gaia* DR2 data. S-SD, DJL, AdB, AHD and JMA acknowledges support from the Spanish Government Ministerio de Ciencia, Innovación y Universidades through grants PGC2018-095 049-B-C22 and PGC-2018-091 3741-B-C22. JIGH acknowledges financial support from the Spanish Ministry of Science, Innovation and Universities (MICIU) under the 2013 Ramón y Cajal program RYC-2013-14875. JIGH and CAP acknowledge financial support from the Spanish Ministry project MICIU AYA2017-86389-P. SJS acknowledges funding from STFC Grant ST/P000312/1. Based on observations made with the Telescopio Nazionale Galileo (TNG) and the Gran Telescopio Canarias (GTC), installed at the Spanish Observatorio del Roque de los Muchachos of the Instituto de Astrofísica de Canarias, in the island of La Palma. This research has made use of the Keck Observatory Archive (KOA), which is operated by the W. M. Keck Observatory and the NASA Exoplanet Science Institute (NEXSci), under contract with the National Aeronautics and Space Administration. Guoshoujing Telescope (the Large Sky Area Multi-Object Fiber Spectroscopic Telescope LAMOST) is a National Major Scientific Project built by the Chinese Academy of Sciences. Funding for the project has been provided by the National Development and Reform Commission. LAMOST is operated and managed by the National Astronomical Observatories, Chinese Academy of Sciences.

References

- Abdul-Masih et al. 2019, arXiv e-prints, arXiv:1912.04092
- Andrews, J. J., Breivik, K., & Chatterjee, S. 2019, *ApJ*, 886, 68
- Bailer-Jones, C. A. L. et al. 2018, *AJ*, 156, 58
- Belczynski, K. et al. 2019, arXiv e-prints, arXiv:1911.12357
- Brott, I., de Mink, S. E., Cantiello, M., et al. 2011, *A&A*, 530, A115
- Cutri, R. M. & et al. 2013, *VizieR Online Data Catalog*, 2328
- Ekström, S., Georgy, C., Eggenberger, P., et al. 2012, *A&A*, 537, A146
- El-Badry, K. & Quataert, E. 2019, arXiv e-prints, arXiv:1912.04185
- Eldridge, J. J. et al. 2019, arXiv e-prints, arXiv:1912.03599
- Evans, D. W., Riello, M., De Angeli, F., et al. 2018, *A&A*, 616, A4
- Groh, J. H., Farrell, E., Meynet, G., et al. 2019, arXiv e-prints, arXiv:1912.00994
- Hempel, M. & Holweger, H. 2003, *A&A*, 408, 1065
- Henden, A. A. et al. 2015, in *AAS Abstracts #225*, 336.16
- Lanz, T. & Hubeny, I. 2007, *ApJS*, 169, 83
- Lindgren, L. et al. 2018a, *A&A*, 616, A2
- Lindgren, L. et al. 2018b, https://www.cosmos.esa.int/documents/29201/1770596/Lindgren_GaiaDR2_Astrometry_extended.pdf
- Liu, J. et al. 2019, *Nature*, 575, 618
- Maíz Apellániz, J. 2001, *AJ*, 121, 2737

³ We have checked that the change in Si abundance or overall metallicity have no significant impact on T_{eff} and $\log g$, that were initially determined with solar abundances.

- Maíz Apellániz, J. 2004, *PASP*, 116, 859
Maíz Apellániz, J. 2006, *AJ*, 131, 1184
Maíz Apellániz, J. 2013, in *HSA7*, 657–657
Maíz Apellániz, J. & Barbá, R. H. 2018, *A&A*, 613, A9
Maíz Apellániz, J., Evans, C. J., Barbá, R. H., et al. 2014, *A&A*, 564, A63
Maíz Apellániz, J. & Pantaleoni González, M. 2018, *A&A*, 616, L7
Maíz Apellániz, J., Sota, A., Walborn, N. R., et al. 2011, in *HSA6*, 467–472
Maíz Apellániz, J. & Weiler, M. 2018, *A&A*, 619, A180
Maíz Apellániz, J. et al. 2018, *A&A*, 616, A149
Mermilliod, J.-C., Mermilliod, M., & Hauck, B. 1997, *A&AS*, 124, 349
Munari, U., Sordo, R., Castelli, F., & Zwitter, T. 2005, *A&A*, 442, 1127
Nieva, M. F. & Simón-Díaz, S. 2011, *A&A*, 532, A2
Puls, J., Urbaneja, M. A., Venero, R., et al. 2005, *A&A*, 435, 669
Reid, M. J., Menten, K. M., Brunthaler, A., et al. 2014, *ApJ*, 783, 130
Schneider, F. R. N., Langer, N., de Koter, A., et al. 2014, *A&A*, 570, A66
Schönrich, R., Binney, J., & Dehnen, W. 2010, *MNRAS*, 403, 1829
Shen, R. F. et al. 2019, *arXiv e-prints*, arXiv:1911.12581
Simón-Díaz, S. & Herrero, A. 2014, *A&A*, 562, A135
Skrutskie, M. F., Cutri, R. M., Stiening, R., et al. 2006, *AJ*, 131, 1163

-
- ¹ Instituto de Astrofísica de Canarias, E-38 200 La Laguna, Tenerife, Spain
² Universidad de La Laguna, Universidad de La Laguna, E-38 205 La Laguna, Tenerife, Spain
³ Centro de Astrobiología, ESAC campus, Villanueva de la Cañada, E-28 692, Spain
⁴ Leibniz-Institut für Astrophysik Potsdam (AIP), An der Sternwarte 16, 14 482 Potsdam, Germany
⁵ Nordic Optical Telescope, Rambla José Ana Fernández Pérez 7, E-38 711 Breña Baja, Spain
⁶ Astrophysics Research Centre, School of Mathematics & Physics, Queen’s University, Belfast, BT7 1NN, UK

Appendix A: Balmer line profiles

A major difference in the present analysis compared to Liu et al. (2019) is the determination of parameters that imply a significantly lower mass, provided the B-star is a normal main sequence object. In the course of this work we noted an apparent difference between the wings of the Balmer lines in Fig. 1b of Liu et al. (2019), obtained from Keck HIRES data, and those presented here. In particular we note that their $H\delta$ line profile appears to be much narrower than in our data. This is most easily seen by comparing the red wing of $H\delta$ around the region of the $He\ I$ line at 4121\AA (middle panel of Fig. A.1). While the good agreement between our various observations shown in Fig. A.1 lends support to our data reduction processes it is worth recalling the difficulties entailed in normalizing the Hydrogen Balmer lines, in particular as observed with echelle spectrographs. In the relevant temperature and gravity range the pressure sensitive wings of these lines are extremely broad, and cover all of an echelle order in Keck/HIRES⁴, as shown in the upper panel of Fig. A.1. This order contains $H\delta$ and extends from approximately 4060 to 4134\AA , and at no point in this interval does the theoretical profile reach the continuum for any of the models discussed in this paper. At best they reach 99% of the continuum and at worst 97.5%. Therefore if normalization of the profile is performed within this spectral range then care must be taken to treat the theoretical profiles in a consistent manner. In order to derive normalized Balmer line profiles from the Keck/HIRES data we first approximate the blaze function by interpolating between neighbouring orders (in pixel space). The result is an approximately normalized order and any residual slope is removed by fitting a straight line through line-free regions, being careful not to define continuum points within $\pm 20\text{\AA}$ of line center. Theoretical Balmer line profiles are normalized in the same way (cf Fig. A.1, middle panel).

Appendix B: Spectral classification

We review the spectral classification of the B star by first degrading the HARPS-N spectrum to the typical classification resolution of $R \sim 2500$, which is very important for such a sharp lined star. We compare a normalized spectrum with a grid of spectral classification standards, in this case a blue-violet grid developed with data from the Galactic O-Star Spectroscopic Survey (GOSSS, Maíz Apellániz et al. 2011) that includes standards in the spectral type range O2-A0 and in the luminosity class range Vz-Ia+. A comparison with the low-rotation B6 V standard β Sex reveals nearly identical $He\ I\ \lambda 4471$ and $Mg\ II\ \lambda 4481$ profiles and similar $He\ I$ and $C\ II$ lines in general, establishing the spectral subtype at B6. On the other hand, the $H\gamma$ and $H\delta$ profiles are narrower than those of β Sex and similar to those of the B6 IV standard, leading to a luminosity class of IV. LB-1 shows an obvious emission component in the $H\beta$ profile and the metal lines are very narrow (even slightly narrower than those of β Sex). There are no other strong differences with β -Sex (other than the DIBs associated with the higher extinction toward LB-1). Therefore, the spectral type is B6 IVe, significantly later than the B3 V classification proposed by Liu et al. (2019). We also note that their luminosity class of V is incompatible with their preferred $\log g = 3.3$, as B3 V stars have values around 4.0.

⁴ Or even extend into two consecutive orders, as is the case of the HARPS-N spectrum, for which the boundary between the two orders is located $\sim 4085\text{\AA}$, making it even more difficult the blaze correction and normalization process.

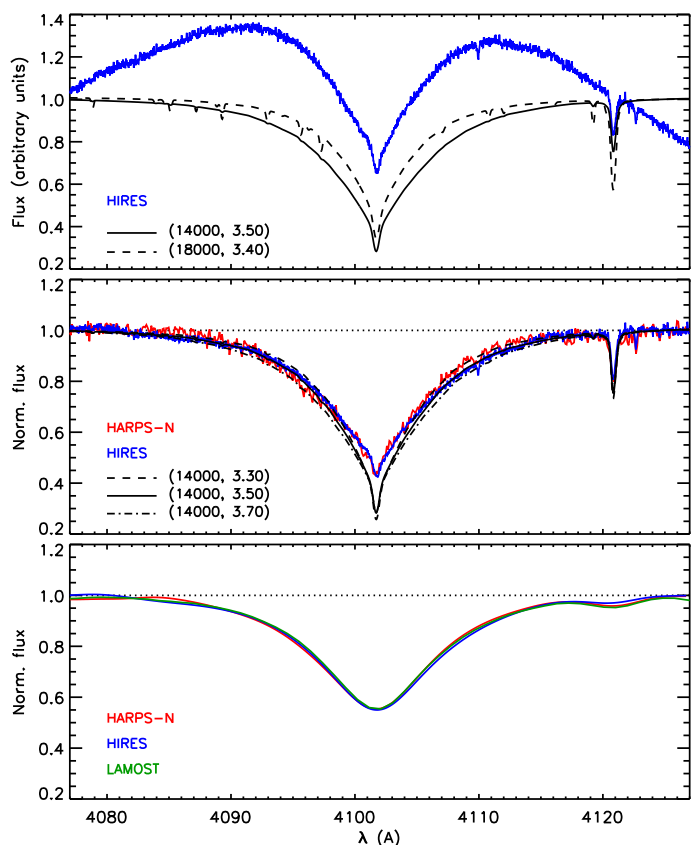


Fig. A.1. Top panel: The blue line is the scaled extracted echelle order from Keck/HIRES, the black continuous and dashed lines are the FASTWIND profiles for the indicated parameters. Middle panel: Blue and red lines are the line profiles normalized using the procedure discussed in the text of Appendix A, while the black lines illustrate the effect of a change of ± 0.2 dex in $\log g$ at constant T_{eff} . Bottom panel: Here we compare the smoothed, normalized profiles for TNG/HARPS-N, Keck/HIRES and LAMOST, illustrating the good consistency obtained for all three datasets.

Appendix C: CHORIZOS analysis

We have used the latest version of the CHORIZOS (Maíz Apellániz 2004) photometry-fitting code to derive some of the parameters of LB-1. We have done two sets of runs and we start describing the first one.

Photometric data. For the first set of runs we collected the magnitudes from *Gaia* DR2 $G + G_{BP} + G_{RP}$ (Evans et al. 2018 with the corrections and calibration from Maíz Apellániz & Weiler 2018), APASS $B + V$ (Henden et al. 2015 with the calibration from Maíz Apellániz 2006), 2MASS $J + H + K_s$ (Skrutskie et al. 2006 with the calibration from Maíz Apellániz & Pantaleoni González 2018), and WISE $W1 + W2 + W3 + W4$ (Cutri & et al. 2013). As the object has a significant IR excess, we eliminate from the runs the five photometric points with the longest effective wavelengths (K_s and the four WISE bands) but include them in the analysis to evaluate the excess.

Models. We use a T_{eff} -luminosity class grid with solar metallicity from Maíz Apellániz (2013). The temperature of interest lies at the transition region between the TLUSTY (Lanz & Hubeny 2007) and Munari (Munari et al. 2005) parts of the grid, so data from both sources are used. In particular, note that the NIR colors from TLUSTY models for late/mid-B stars are incorrect by up to several hundredths of a magnitude, so in that

region of the spectrum the grid uses the Munari models for all hot stars.

Parameters. For the first set of runs we fix T_{eff} to 14 kK from the results in this paper and we do four individual runs for different values of the luminosity class: 5.5 (ZAMS), 5.0 (typical class V), 4.5 (luminosity class V), and 4.0 (typical class IV). The corresponding values of $\log g$ (in cgs) are 4.27, 4.04, 3.59, and 3.38; of the initial stellar mass (in M_{\odot}) are 3.6, 4.2, 4.9, and 5.8; and of the evolutionary age (in Ma) are 0, 85, 111, and 75. We leave the two extinction parameters free: $E(4405 - 5495)$ (amount of extinction) and R_{5495} (type of extinction) and we use the family of extinction laws of Maíz Apellániz et al. (2014). See Maíz Apellániz (2004); Maíz Apellániz & Barbá (2018) for an explanation of why one needs to use monochromatic quantities instead of band-integrated ones to characterize extinction. We also leave $\log d$ free, yielding a total of three free parameters to be fitted in each of the four runs. As we are fitting seven photometric points we have four degrees of freedom.

Results. All four runs yield excellent values of the reduced χ^2 around 0.6, indicating that the model SEDs are consistent with the observed photometry. The values for the extinction parameters are very similar for the four runs, which was expected because broad-band colors to the right of the Balmer jump are a very weak function of gravity for B stars. We obtain $E(4405 - 5495) = 0.413 \pm 0.013$ and $R_{5495} = 3.60 \pm 0.16$. Note that the value for the amount of extinction is significantly lower than the one Liu et al. (2019) obtains but as R_{5495} is also higher than the canonical value of 3.1 there is little change in A_V . This deviation from the canonical extinction law towards higher values is typical of low-extinction environments; only for higher extinctions the canonical value becomes the more common one (Maíz Apellániz & Barbá 2018), which is why it is dangerous to assume a value of R_{5495} instead of actually measuring it. The main difference between the four runs are the values of $\log d$, which are (in log pc), respectively, 2.975, 3.116, 3.380, and 3.520. Note that for luminosity class 4.5 (third run) we obtain a distance close to 2 kpc (close to the *Gaia* DR2 value) which corresponds to a value of $\log g$ close to 3.6 (cgs), a mass around 5 M_{\odot} , and an age around 110 Ma. Therefore, the photometric-based CHORIZOS analysis leads to a result consistent with the spectroscopic analysis in this paper.

For the second set of runs we use the same photometry as before but we add a Johnson *U* magnitude by combining the *U - B* color from Mermilliod et al. (1997) with the APASS *B* magnitude. This allows us to leave T_{eff} as a free parameter, as the Balmer jump provides an accurate measurement of that quantity for OB stars if the extinction law is well characterized (Maíz Apellániz et al. 2014). In this case we do a first run with a luminosity class of 5.0 leaving the two extinction parameters and $\log d$ free and a second run where we change the luminosity class to 4.0. This leaves in each run four free parameters and eight photometric points i.e. four degrees of freedom.

The first run of the second set has a reduced χ^2 of 0.50. The values of the extinction parameters are within 1.5 sigmas of the previous ones, $E(4405 - 5495) = 0.443 \pm 0.023$ and $R_{5495} = 3.63 \pm 0.14$, and $\log d = 3.219 \pm 0.048$ log pc is also similar to the previous equivalent result. The important result of this run is that we find $T_{\text{eff}} = 16500 \pm 1100$ K, which is relatively close to the value obtained from the spectroscopic analysis and to the value expected for a B6 IV star. This implies that the contribution of the disk to the optical continuum is small because if it were not the Balmer jump would be reduced and we would obtain a significantly hotter temperature. Another piece of indirect evidence in the same direction are the excellent values

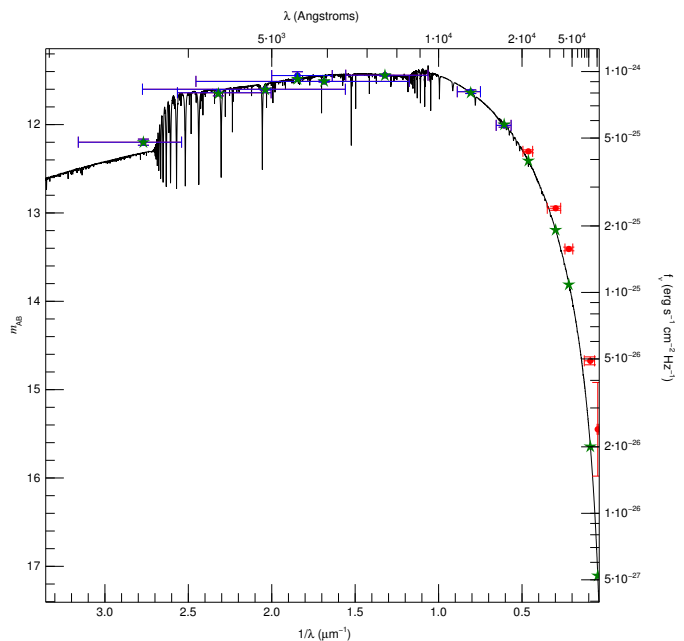


Fig. C.1. Best-fit SED for the first run of the second CHORIZOS set. Green stars indicate model photometry, blue symbols and error bars indicate input photometry used for the fit, and red symbols and error bars indicate input photometry not used for the fit.

of the reduced χ^2 of all runs, as a significant non-stellar continuum would push the photometric solution out of the parameter space covered by the stellar models. We show in Fig. C.1 the photometry and best-fit SED. In that Figure it is clear there is a significant infrared excess as a likely result of the disk contribution. For the best-fit SED the excess is 0.107 ± 0.017 mag at K_s and 0.971 ± 0.045 at $W3$. At $W4$ the input uncertainty is very large but the excess is already close to 2 mag.

The second run of the second set yields very similar results to the first one except for T_{eff} and $\log d$. For the first we get 15700 ± 1100 K, within one sigma of the previous value and even closer to the spectroscopic one. The small difference indicates, in any case, that the T_{eff} value depends only weakly on the luminosity (or gravity). $\log d$, on the other hand, is significantly larger (3.578 ± 0.038 log pc), as expected, falling outside the range of the *Gaia* DR2 value.

Appendix D: *Gaia* DR2 data of LB-1

In this Appendix we analyze the *Gaia* DR2 results for LB-1. We start with the parallax $\varpi = 0.4403 \pm 0.0856$ mas. The corresponding Bailer-Jones et al. (2018) distance is 2140^{+510}_{-310} pc. If we use instead the prior described by Maíz Apellániz (2001) which is more appropriate for early-type stars in the Galactic disk, and a parallax zero point of -0.040 ± 0.010 mas we obtain the alternative similar distance of 2200^{+490}_{-350} pc. The proper motion of LB-1 is nearly exactly southwards, as the value in right ascension is -0.067 ± 0.112 mas/a and the value in declination is -1.889 ± 0.088 mas/a. From the *Gaia* DR2 astrometric point of view, our target is then a typical disk object at a distance of ~ 2 kpc with a typical proper motion for that population, as those values are close to the average for OB stars at its Galactic longitude (Maíz Apellániz et al. 2018).

Going beyond those basic results, we may ask ourselves: is there a sign of the motion of the B star around the black hole in the *Gaia* DR2 data? We can use the results from the Liu et al.

(2019) spectroscopic SB1 orbit to calculate the motion in the plane of the sky. For an edge-on ($\sin i = 1$) orbit, the B star moves back and forth along a line with a semi-amplitude of $a_0 = 0.19$ (2 kpc/d) mas, that is, 38% of the amplitude caused by Earth's motion as measured in *Gaia* DR2. If the orbit is not edge-on, the trajectory is an ellipse with semi-major axes of $a_0/\sin i$ and $a_0/\tan i$, respectively. Note that for a star with $G = 11.4$ the precision for an along-scan position measurement is ≈ 0.3 mas (Lindegren et al. 2018a). From those values it is clear that already for the edge-on case one should see an effect of the motion of the B star around the black hole. For an orbit with a smaller inclination the effect should be even larger and for low enough inclinations it should dominate over the effect of the Earth's motion. However, as the orbital motion is in an arbitrary direction with respect to that of the Earth's orbit and the period is much shorter than one year, the effect in the DR2 astrometric solution should appear as noise, not as signal. In order to actually measure the orbit of the B star around the black hole using *Gaia* data one needs access to the individual epochs, something that is not available in the current release but that will become available in the future (see e.g. Andrews et al. 2019). Therefore, for the time being we have to work with the available limited information.

Despite our calculations in the previous paragraph, *there is no sign of such an orbital motion in the Gaia DR2 data*. We can see this in two ways. First, the RUWE parameter (Lindegren et al. 2018b), which is the recommended goodness-of-fit for *Gaia* DR2 astrometry, is 0.91, close to the ideal value of 1 and much lower than the suggested critical value of 1.4. Second, *Gaia* DR2 attempted to use 103 along-the-scan observations and only discarded three, indicating that there were very few outliers to the fit⁵. Therefore, we face a conundrum: if the only significant contribution to the *G* band photometry, and hence astrometry, in the system comes from the B star and the Liu et al. (2019) spectroscopic orbit is correct, what is going on with the *Gaia* astrometry? We believe that the issue has to do with the special circumstances of this system. First, LB-1 is located very close to the northernmost point of the ecliptic, which results in the reflex motion of the star due to the Earth's motion being in an east-west line instead of in a true ellipsoid. Second, the proper motion of the star is in a nearly perpendicular direction (close to the north-south direction) to that. Therefore, ignoring the effect of the BH the trajectory of the star in the sky is close to a sinusoid, as opposed to the complex trajectories that usually result of the sum of a linear motion with an arbitrary velocity (proper motion) and an ellipse whose shape is determined by the position in the sky and its amplitude by its parallax. In other words, it is a case where the fit parameters are degenerate and subject to peculiar results when perturbations are included. In this particular case, we propose that *if the B-star orbit has indeed a very high inclination with its axis pointing in a near east-west direction, Gaia would detect little excess noise in the parallax measurements* and would only see the star slowing down and speeding up in the proper motion direction, something that may not come up as excess noise in the output. The most critical aspect is the high inclination, as a lower value would make the orbit span a larger angular size in the sky that would be harder to miss by *Gaia*. In this respect, we point out that even though in *Gaia* DR2 there are 12 epochs observed, three of them are actually close in time to others and there are only nine real visibility periods employed

in the solution, so it is not far-fetched to think that the orbital motion would have been missed if the system is in the proposed configuration. The answer should come in future releases when more epochs are included in the solution and information from individual epochs becomes available. In the meantime, it would be useful to make polarization observations in $H\alpha$ to see if the proposed circumbinary disk is indeed oriented this way.

If the hypothesis in the paragraph above (or a slightly modified version of it) turns out to be true, there are two interesting consequences for LB-1. The first one is that a high inclination in the spectroscopic orbit results in a significantly lower mass for the black hole. If the B star has a mass of $5 M_\odot$, for $\sin i = 1$ we are left with a black hole of only $4.9 M_\odot$ (for $\sin i = 0.7$ its mass becomes $8.6 M_\odot$ and for $\sin i = 0.4$, $26.1 M_\odot$). If the B star has instead a mass of $3 M_\odot$, the minimum mass of the BH is just $3.8 M_\odot$. The second one is that, as we have measured a very low rotational $v \sin i$ for the B star, either v is really very low (the star is a true slow rotator) or its rotation axis points in a near-perpendicular direction with respect to its orbital axis.

⁵ A possible third way to detect this would be through the excess astrometric noise but that should not be used for a bright star like this one due to the problems associated with the ‘‘DOF bug’’, see appendix A in Lindegren et al. (2018a).